DSMC Aero-Thermo-Dynamic Analysis of a Deployable Capsule for Mars Entry

G. Zuppardi – R. Savino

Department of Industrial Engineering – Aerospace Division
University of Naples "Federico II"
Piazzale Tecchio, 80 – 80125 Naples, Italy
zuppardi@unina.it

Abstract: A deployable capsule is made of flexible, high temperature resistant fabric, folded at launch and deployed in space at the beginning of the re-entry. This kind of capsule thanks to lightness and to low costs can be an alternative to the current "conventional" capsules. The present authors already analyzed the trajectory and the aerodynamic behavior of such a kind of capsule during the Earth re-entry. In that study an aerodynamic longitudinal stability analysis and an evaluation of the thermal and mechanical loads for a possible, suborbital re-entry demonstrator, was carried out in both continuum and rarefied regimes. The results verified that a stable equilibrium condition is verified around the zero angle of attack and an unstable equilibrium condition is verified around the 180 angle of attack; therefore the capsule turned out to be self-stabilizing. In the present paper the trajectory, the longitudinal stability, the thermal and mechanical loads of the same capsule has been evaluated for a possible use in Mars entry. The present study is aimed at providing preliminary information considering both the diversity of the two atmospheres and the diversity of the two types of entry: ballistic, sub-orbital for Earth, direct for Mars and therefore of the initial entry velocity. The parameters were compared with those along the Earth re-entry. As the computer tests have been carried out at high altitudes, therefore in rarefied flow fields, the use of Direct Simulation Monte Carlo codes has been mandatory. The computations involved both global aerodynamic quantities (drag and longitudinal moment coefficients) and local aerodynamic quantities (heat flux, pressure and skin friction distributions along the capsule surface). The results verified that the capsule at high altitude (100 km) in Mars entry is not self-stabilizing; it is stable both around the nominal attitude or at zero angle of attack and around the reverse attitude or at 180 deg angle of attack. Furthermore, due to the much higher entry velocity, the local quantities are of several orders of magnitude higher than the ones in Earth re-entry.

1. Introduction

It is well known that a deployable, or umbrella like, re-entry capsule, thanks to lightness, to low costs of construction and of management, can be an alternative to the current "conventional" capsules. In fact, a deployable capsule is made of flexible, high temperature resistant fabric, folded at launch and deployed in space at the beginning of the re-entry for de-orbit and for other re-entry operations. Reducing size, mass and power implies a significant reduction of launch costs and an increment of management capability and finally an increment of accessibility to space.

The present authors already analyzed the trajectory and the aerodynamic behavior of such a kind of capsule during the Earth re-entry [1]. In that study, the capsule was supposed to be carried by a relatively small and low energy sounding rocket (for example low energy sounding rockets, suitable for such a purpose, are REXUS and MAPHEUS [2], launched from the Esrange Space Center in Kiruna, Sweden) and then ejected around its trajectory apogee (about 100 km) after the motor burn-out. Then, during the descending leg of the parabola, the aero-brake is completely deployed and the capsule, thanks to an increment of the ballistic parameter B (defined as the ratio between the base area of the capsule times the drag coefficient and its mass) therefore thanks to a decrement of velocity, performs an atmospheric entry with reduced thermal and mechanical loads. More specifically in that study, an aerodynamic longitudinal stability analysis and an evaluation of the thermal and mechanical loads for a possible, suborbital re-entry demonstrator, have been made in both continuum and rarefied regimes.

The results verified that the capsule is aerodynamically self-stabilizing; the equilibrium is stable around the nominal attitude at zero angle of attack and is unstable around the nominal attitude at 180 angle of attack. This can ensure that the capsule does not assume, at high altitudes, a wrong attitude during the re-entry and the effectiveness of the system is not compromised. In this case, in fact, its axis is always aligned with the free stream velocity thus

the stagnation point lies on the nose. This is a very important requirement considering that the deployable capsules are not provided with any attitude active control systems.

In the present study, the trajectory, the longitudinal stability, the thermal and mechanical loads of the same capsule, already evaluated for Earth re-entry [1], has been evaluated for Mars entry. The present study is aimed at providing preliminary information considering the differences of both the two atmospheres and the two types of entry (ballistic, sub-orbital for Earth and direct for Mars) therefore of the initial entry velocity. The parameters were compared with those along the Earth re-entry. As the computer tests have been carried out at high altitudes therefore in rarefied flow fields, the use of Direct Simulation Monte Carlo codes has been mandatory. The computations involved both global aerodynamic quantities, such as drag and longitudinal moment coefficients, and local aerodynamic quantities, such as heat flux, pressure and skin friction distributions along the capsule surface.

2. Re-entry demonstrator configuration

The present re-entry demonstrator [1] consists of a cylinder containing the payload and all subsystems necessary for the mission, umbrella-like framework, ceramic fabric for the conical deployable aero-brake and a light-weight, temperature-resistant material (e.g. carbon fiber composites) for the rigid hemispherical nose. Subsystems could include: Inertial Measurement Unit (IMU), batteries and sensors, depending on the mission objectives. A total re-entry mass of 15 kg has been assumed.

Figure 1 shows the investigated geometrical configuration. When completely deployed, the aero-brake forms a half cone angle of 45 deg and a maximum diameter (D) of 0.9 m is achieved. On the other hand, the cylindrical payload bay has a diameter of 0.2 m and a total length of 0.21 m. The capsule is also provided with a rigid hemispherical nose (0.04 m thick). When the aero-brake is completely deployed, the nose moves ahead to ensure the umbrella-like framework rotation up to the final configuration (thus the total length of the capsule increases to 0.35 m). The drag and moment coefficients are computed considering as reference area the base area (0.66 m^2) and as reference length the longitudinal dimension (0.40 m) of the aero-brake in deployed configuration. Table 1 summarizes some parameters of the re-entry demonstrator. The reference system has been assumed according to Fig. 1, being the z-axis such as to form a right-handed triad with the longitudinal x-axis and the radial y-axis.

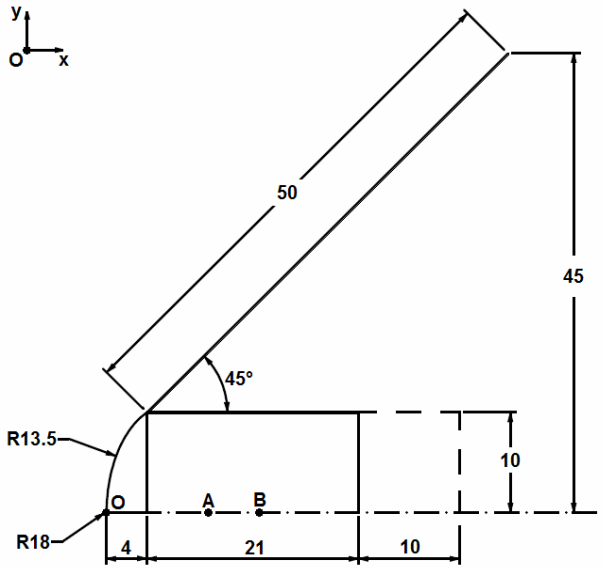

Fig. 1. Geometrical characteristics of the re-entry demonstrator (dimensions are in centimeters)

Table 1 – Parameters of re-entry demonstrator

Cylinder length [m]	0.21 ÷ 0.35
Cylinder diameter [m]	0.20
Mass [kg]	15.0
Base diameter [m]	0.92
Reference surface [m^2]	0.66
Nose radius [m]	0.18
Reference length [m]	0.40
Base area [m^2]	0.66

3. Mars and Earth atmosphere

The parameters of the Mars atmosphere are computed by means of the NASA "Mars Atmosphere model". According to this model, pressure (p) decreases exponentially with altitude (h):

$$p = 0.699 \exp(-0.00009\ h) \tag{1.a}$$

Temperature (T) decreases linearly. For the computation of temperature, the Mars atmosphere is divided in two zones: a lower zone up to 7000 m and an upper zone for higher altitudes. Temperature is evaluated by the following equations:

$$h \leq 7000\ \text{m}: T = -31 - 0.000998\ h \tag{1.b}$$

$$h > 7000\ \text{m}: T = -23.4 - 0.00222\ h \tag{1.c}$$

where temperature is in Celsius degrees, pressure is in kilo-Pascals and altitude is in meters. In each zone, density (ρ [kg/m^3]) is computed by the equation of state:

$$\rho = p / [0.1921\ (T + 273.1)] \tag{1.d}$$

The composition of the Mars atmosphere is supposed constant with altitude. Table 2 reports both the mass and the molar fractions of each chemical species.

Table 2 – Mars atmosphere chemical composition

Chemical species	Mass fraction	Molar fraction
O_2	0.0013	0.00176
N_2	0.0270	0.04173
NO	0.0001	0.00014
CO	0.0007	0.00108
CO_2	0.9500	0.93399
Ar	0.0160	0.01734

The Earth atmosphere parameters are computed by a computer version of the "US standard Atmosphere 1976 model". Figures 2(a) and 2(b) show the profiles of density and temperature. For completeness Figures 2(c) and 2(d) show the profiles of the number density (N [m^{-3}]) and of the Knudsen number of the present capsule ($Kn_{\infty D}=\lambda_\infty/D$, λ_∞ is the free stream mean free path). In both atmospheres and in the altitude interval 60-100 km, the capsule meets a rarefied regime; according to Moss [3], the transitional regime is defined by $10^{-3}<Kn_{\infty D}<50$.

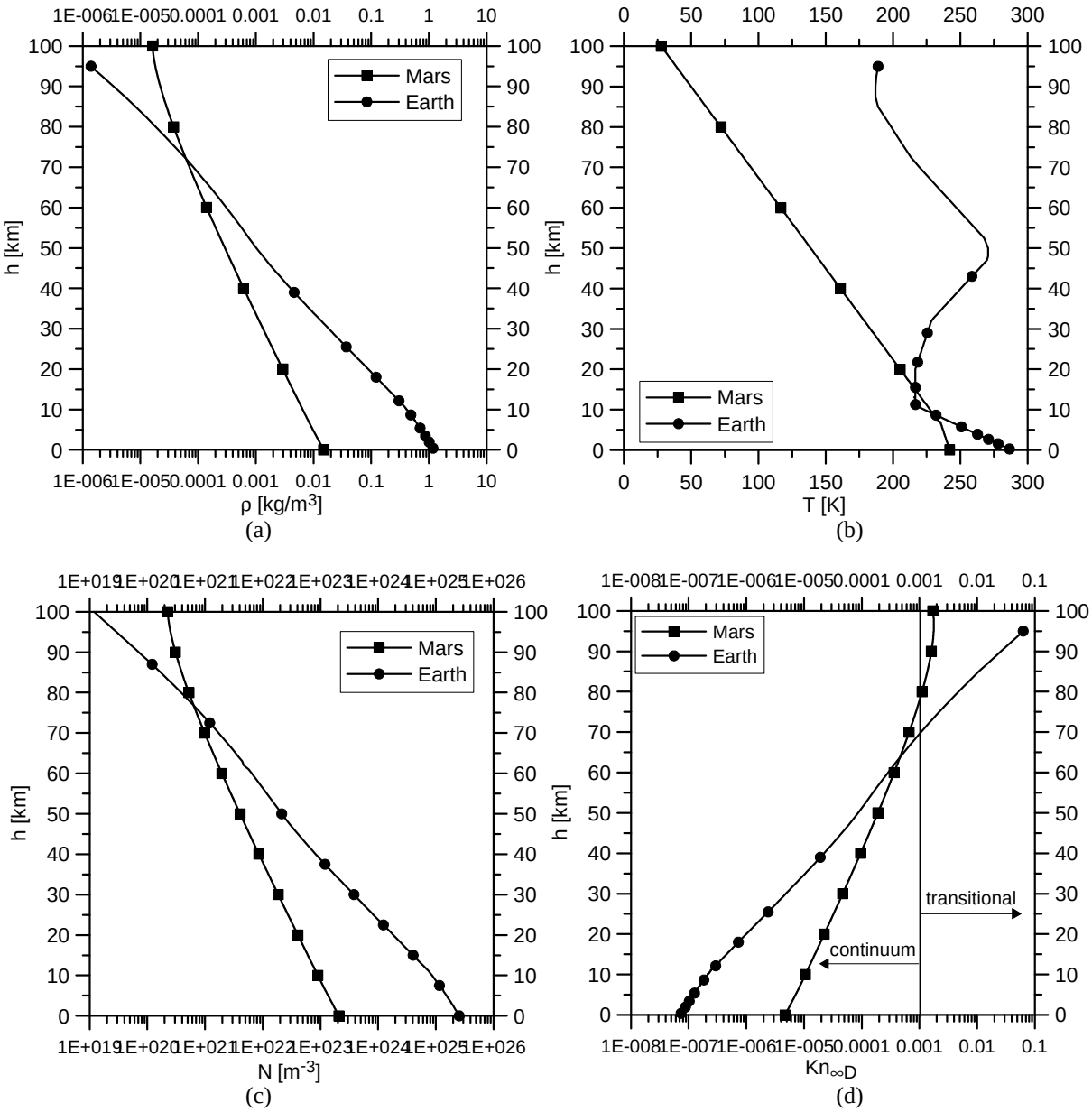

Fig. 2 – Profiles of density (a), temperature (b), number density (c) and re-entry demonstrator free stream Knudsen number of Mars and Earth atmosphere

4. Mars and Earth re-entry trajectories

Equations 2.a and 2.b compute dynamics of the capsule:

$$\frac{dV}{dh} = \frac{1}{2}\frac{\rho V}{\sin\gamma}\frac{SC_D}{m} - \frac{g}{V} \tag{2.a}$$

$$\frac{d\gamma}{dh} = \frac{1}{R\sin\gamma} - \frac{g}{V^2}\frac{1}{tg\gamma} \tag{2.b}$$

where V is the velocity, γ is the flight path angle, C_D is the drag coefficient, S is the capsule base area, m is the capsule mass, g is the gravity acceleration and R is the curvature radius of the trajectory. The pressure at the stagnation point (p(0)) has been evaluated assuming a pressure coefficient equal to 2 thus:

$$p(0) \cong \rho V^2 \tag{3.a}$$

whereas the stagnation point convective heat flux ($\dot{q}(0)$) has been evaluated by the Tauber's engineering formula [4]:

$$\dot{q}(0) = 1.83 \times 10^{-4} \sqrt{\frac{\rho}{r}} V^3 \tag{3.b}$$

where r is the radius of curvature of the capsule nose at the stagnation point.

Equations 2(a), (b) have been integrated numerically by a forward scheme with a first order approximation (Euler method). For a preliminary analysis, the aerodynamic drag coefficient has been assumed equal to 1. The initial conditions are:

h=96 km: V=260 m/s, γ=0 deg [1] for the Earth ballistic, sub-orbital re-entry (according to typical apogee conditions for the REXUS rocket [5, 6]),

h=100 km: V=4700 m/s, γ=17 deg for the Mars direct entry (according to those of the Viking I/II capsules [7, 8]).

Figures 3(a) to 3(d) show the preliminary re-entry trajectories considered for the present analysis in terms of: free stream velocity (a), free stream Mach number (b), pressure at the stagnation point (c), convective heat flux at the stagnation point (d).

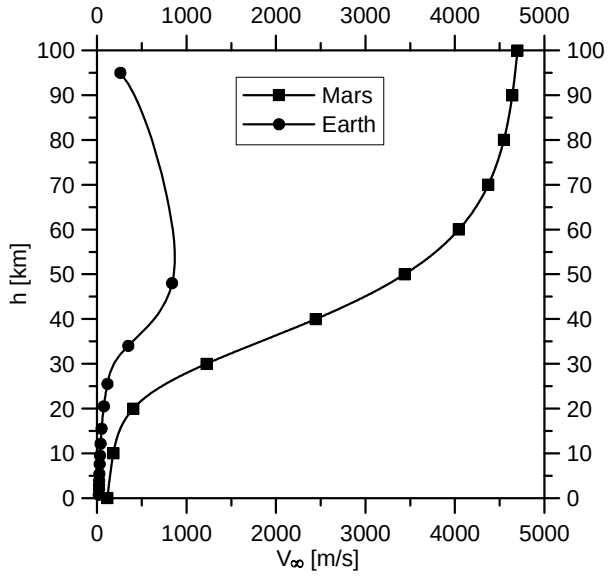

(a)

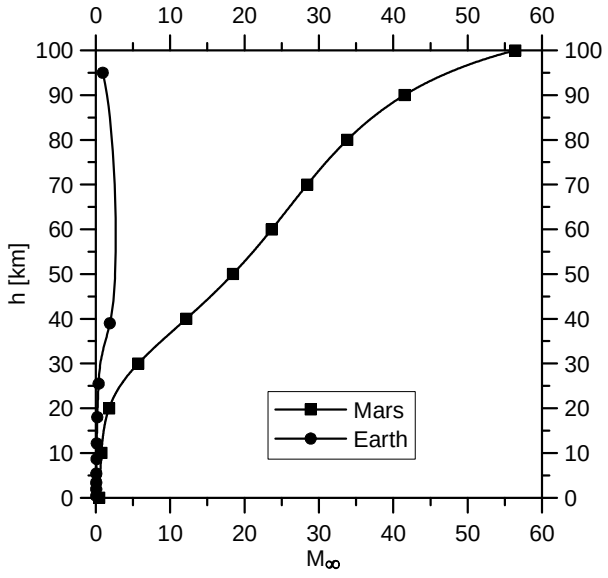

(b)

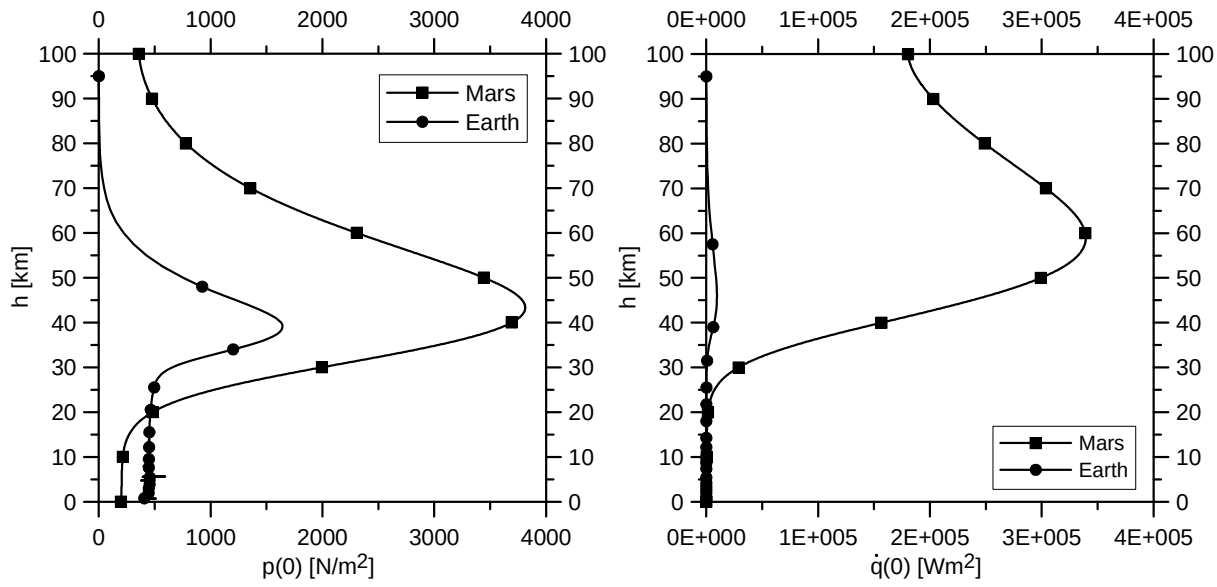

(c) (d)

Fig. 3 – Profiles of velocity (a), Mach number (b), stagnation point pressure (c) and heat flux (d) along the Mars and Earth atmosphere entry

The following Eq. 4 computes the thermal load at the stagnation point of the capsule (Q(0)):

$$Q(0) = \int_0^t \dot{q}(0)dt \tag{4}$$

where t is the travel time of the trajectory. The thermal loads and the travel times for Earth and Mars trajectories are about 3.44×10^2 and 1.60×10^4 [kJ/m^2] and 830 and 242 [s], respectively.

5. Direct Simulation Monte Carlo (DSMC) codes

It is well known that the Direct Simulation Monte Carlo (DSMC) method [9, 10, 11] is currently the only available tool for the solution of rarefied flow fields from continuum low density (or slip flow) to free molecular regimes. DSMC considers the gas as made up of discrete molecules. It is based on the kinetic theory of gases and computes the evolution of millions of simulated molecules, each one representing a large number (say 10^{15}) of real molecules in the physical space. Intermolecular and molecule-surface collisions are also taken into account. The computational domain is divided in cells, used both for selecting the colliding molecules and for sampling the macroscopic, fluid-dynamic quantities. The most important advantage of the method is that it does not suffer from numerical instabilities and does not directly rely on similarity parameters (i.e. Mach and Reynolds numbers). On the other hand, it is inherently unsteady. A steady solution is achieved after a sufficiently long simulated time.

The DSMC codes used in the present study are: 1) 2-D/axial-symmetric DS2V-3.3 [12], 2) 2-D/axial-symmetric DS2V-4.5 64 bits [13], 3) 3-D DS3V-2.6 [14]. The DS2V-3.3 and DS3V-2.6 codes have been used for the Mars simulations. In fact both codes implement the Mars atmosphere, made of 9 species, and consider 59 built-in chemical reactions. Besides the six free stream species, forming the Mars atmosphere (see Table 2), the gas is considered as made up of other 3 species: atomic Oxygen, atomic Nitrogen and Carbon, produced by the chemical reactions. DS2V-4.5 has been used for the Earth simulation. This code considers air as made up of five neutral reacting species (O_2, N_2, O, N and NO) and rely on the built-in Gupta-Yos-Thompson [15] chemical model, consisting of 23 reactions. The 3-D Earth tests by DS3V-2.6 were already run to get the results presented in [1].

All codes are "sophisticated", as widely reported in literature [16, 17, 18], a DSMC code is defined sophisticated if it implements computing procedures able to guarantee a higher efficiency and accuracy with respect to a “basic” DSMC code. A sophisticated code, in fact, considers two sets of cells (collision and sampling cells) with the related cell adaptation and implements methods promoting nearest neighbour collisions. This type of code generates automatically computational parameters such as numbers of cells and of simulated molecules by the input numbers of megabytes and of free stream number density. It uses a radial weighting factor in solving axial-symmetric flow fields and provides optimal time step. Finally, the same collision pair cannot have sequential collisions.

Besides being sophisticated, these codes are also advanced; the user can verify that the number of simulated molecules and collision cells are adequate by the on line visualization of the ratio between the molecule mean collision separation (mcs) and the mean free path (λ) in each collision cell. In addition, the codes allow the user to change (or to increase) during the run the number of simulated molecules. The mcs/λ ratio has to be less than unity everywhere in the computational domain. Bird [16] suggests 0.2 as a limit value for an optimal quality of the run. In addition, the code gives the user information about the stabilization of the runs by means of the profile of the number of simulated molecules as a function of the simulated time. The stabilization of a DSMC calculation is achieved when this profile becomes jagged and included within a band defining the standard deviation.

6. Test conditions and quality of the results

Tables 3 and 4 report some input and free stream parameters for the Mars and the Earth simulations. The Mars 2-D runs have been performed (by DS2V-3.3) at 6 altitudes for the evaluation of the capsule drag coefficient along the re-entry path. The Mars 3-D runs have been performed (by DS3V-2.6) at the two altitudes of h=100 and 80 km and at the angles of attack 0, 5, 10 deg and 170, 175 and 180 deg for evaluating the capsule longitudinal stability. The Earth 2-D run has been carried out (by DS2V-4.5) at the altitude of 80 km for the evaluation of local quantities such as heat flux, pressure and shear stress.

Table 3 Input data and free stream parameters in rarefied flow for Mars simulations

h [km]	V_∞ [m/s]	N_∞ [m^{-3}]	T_∞ [K]	M_∞	$Re_{\infty D}$	$M_\infty/Re_{\infty D}$	$Kn_{\infty D}$
100	4700	2.26×10^{20}	28	56	42533	1.3×10^{-3}	1.7×10^{-3}
90	4642	3.08×10^{20}	50	42	33178	1.3×10^{-3}	1.6×10^{-3}
80	4548	5.24×10^{20}	72	34	39293	8.7×10^{-4}	1.1×10^{-3}
70	4374	9.86×10^{20}	94	28	55368	5.0×10^{-4}	6.6×10^{-4}
60	4044	1.96×10^{21}	117	24	83737	2.9×10^{-4}	3.7×10^{-4}
50	3438	4.06×10^{21}	139	18	125041	1.4×10^{-4}	1.9×10^{-4}

Table 4 Input data and free stream parameters in rarefied flow for Earth simulations

h [km]	V_∞ [m/s]	N_∞ [m^{-3}]	T_∞ [K]	M_∞	$Re_{\infty D}$	$M_\infty/Re_{\infty D}$	$Kn_{\infty D}$
96	260	2.92×10^{19}	189	0.94	25	3.8×10^{-2}	6.3×10^{-2}
80	612	3.84×10^{20}	199	2.2	759	2.9×10^{-3}	4.1×10^{-3}

The DS2V-3.3, DS3V-2.6 and DS2V-4.5 runs have been carried out with a number of simulated molecules of about 2.0×10^7, 9.0×10^6 and 5.0×10^7, respectively. For all runs, the codes suggested a number of 8 molecules/cell for the adaptation process of the collision cells while, for the sampling cells, DS2V-3.3 and DS3V-2.6 suggested a number of 30 molecules/cell and DS2V-4.5 suggests a number of about 250 molecules/cell.

Besides from the above mentioned DSMC criterion (see sec. 5), the stabilization of the runs has been verified also from a fluid dynamic point of view by means of the ratio of the simulated time (t_S) and the time needed to cross the computing region at the free stream velocity (t_f). A rule of thumb suggests considering that a fluid-dynamic computation is reasonably stabilized if $t_S/t_f \cong 10$. As reported in Tables 5, the value of mcs/λ averaged on the computing region for the Mars 2-D runs does not satisfy the suggested limit value of 0.2, it is less than unity up to the altitude of 60 km, as requested by the method and is only slightly higher than 1 at h=50 km. The same remarks hold for the 3-D runs by DS3V-2.6. On the opposite, the run by DS2V-4.5 at h=80 km satisfied completely the criterion proposed by Bird (Table 6). Furthermore, the ratios t_S/t_f satisfy the stabilization criterion of the runs from a

fluid-dynamic point of view. The quality of the DSMC computations can be therefore considered reasonably satisfactory.

Table 5 Quality parameters for the DS2V-3.3 Mars runs

	h=100 km	h=90 km	h=80 km	h=70 km	h=60 km	h=50 km
mcs/λ	0.1	0.2	0.4	0.6	0.8	1.2
t_s/t_f	5.04	6.39	5.10	7.30	7.22	4.61

Table 6 Quality parameters for the DS2V-4.5 Earth runs

	h=80 km
mcs/λ	0.02
t_s/t_f	43

7. Analysis of the results

7.1 DS2V tests

The Mars 2-D tests were aimed at the evaluation of the drag coefficients at zero angle of attack (α=0 deg or in axial-symmetric flow) as a function of altitude and at the evaluation of local quantities such as heat flux, pressure and skin friction along the capsule surface. The Earth 2-D test, for example at h=80 km, was aimed at the evaluation of the distribution of local quantities. Using 2-D codes for the computation of local quantities is appropriate for achieving a better geometrical definition of the body, including a more precise localization of the nose stagnation point.

Figure 4 shows that the capsule drag coefficient ranges, in the altitude interval 50-100 km, from 1.07 to 1.19, therefore not very far from 1. The best fit polynomial curve (Eq.5), providing an excellent match of the drag coefficients, has been used for computing the ballistic parameter in this altitude interval therefore for evaluating the influence of a variable drag coefficient on the re-entry trajectory:

$$C_D = 1.5043 - 0.0197h + 0.0003h^2 - 1.1296h^3 \quad (5)$$

where h is in kilometers. The drag coefficient at altitude lower that 50 km has been left equal to 1.

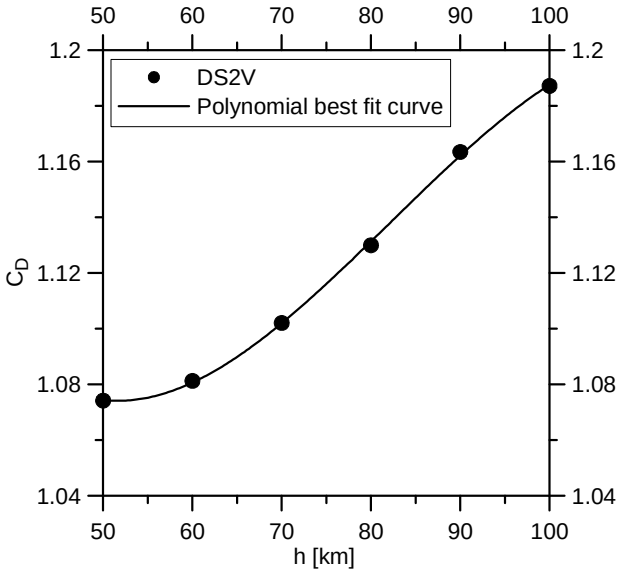

Fig. 4 – Computed drag coefficients and polynomial best fit curve: α=0 deg

Figures 5(a) to 5(d) show the comparison of the re-entry trajectories computed with a constant drag coefficient (C_D=1) and a variable drag coefficient. The small increase of C_D therefore of B, involves a small decrease of velocity therefore of pressure and heat flux. For example, the maximum pressure and heat flux at the stagnation point decrease from 3814 to 3602 [N/m^2] and from 3.39×10^5 to 3.22×10^5 [W/m^2]; the percentage decreases are about 6% and 5%, respectively. Furthermore, the altitudes where the maximum values are met, remain practically the same; h=45 km for pressure and h=60 km for heat flux. The influence of a variable C_D is negligible also on the heat load and the re-entry time. These are comparable with those obtained with C_D=1; in fact $Q(0)=1.54\times10^4$ [kJ/m^2] and t=243 [s].

The much higher velocity, at the beginning of Mars entry, increases strongly the pressure and the convective heat flux at the stagnation point with respect to the same parameters for Earth re-entry. In fact, in the Earth re-entry, the maximum values of p(0) and $\dot{q}(0)$ are 1643 [N/m^2] and 9451 [W/m^2] (see Figs.3(c) and 3(d)). The same remark holds also from the profiles of heat flux, pressure and shear stress along the capsule surface therefore a more resistant fabric, compared with that scheduled for Earth re-entry, should be necessary. For example, these quantities are compared in Figs. 6(a), 6(b), 6(c) with those during the Earth re-entry, at the altitude of 80 km.

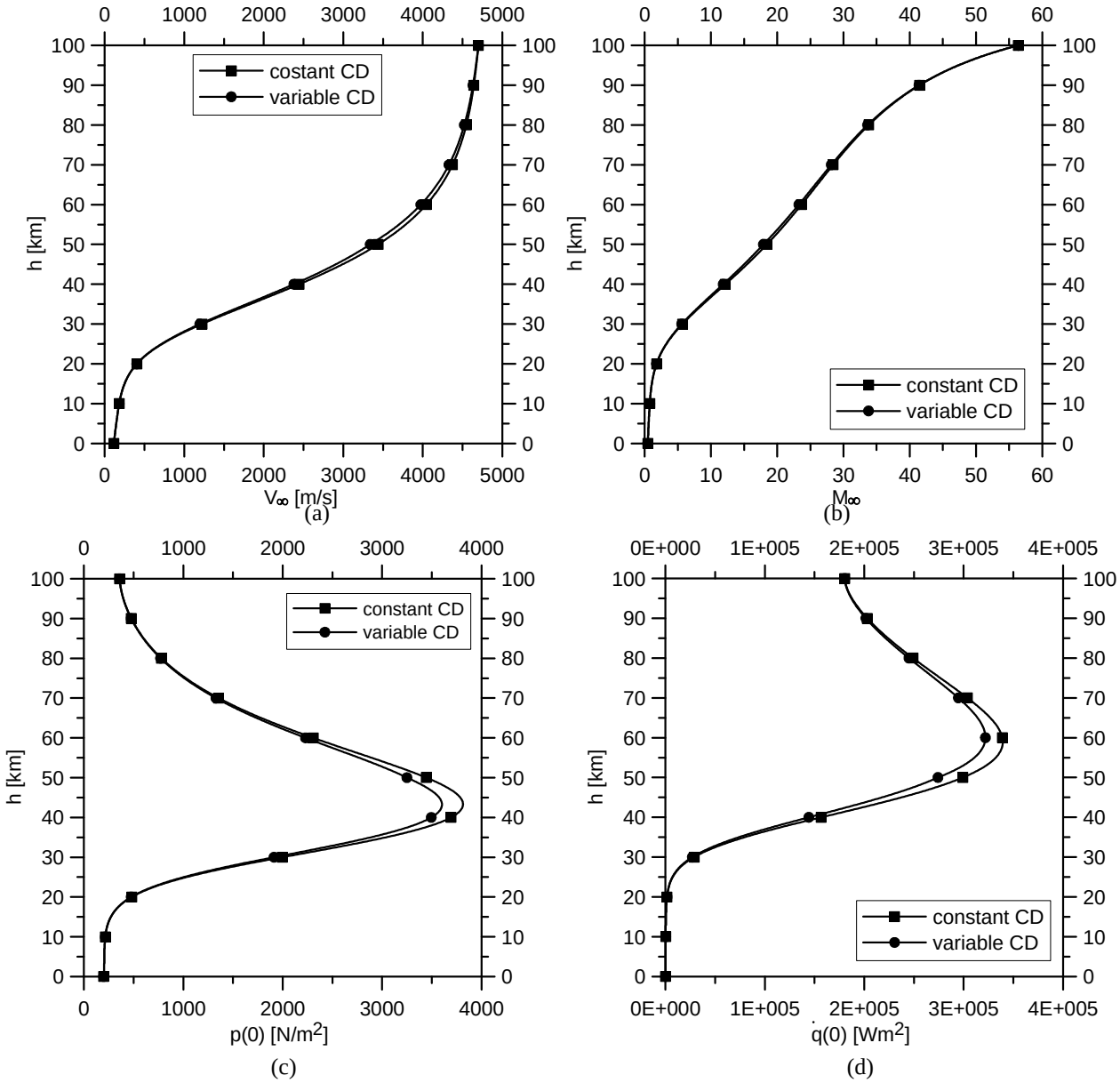

Fig. 5 – Influence of variable drag coefficient on the Mars entry trajectory

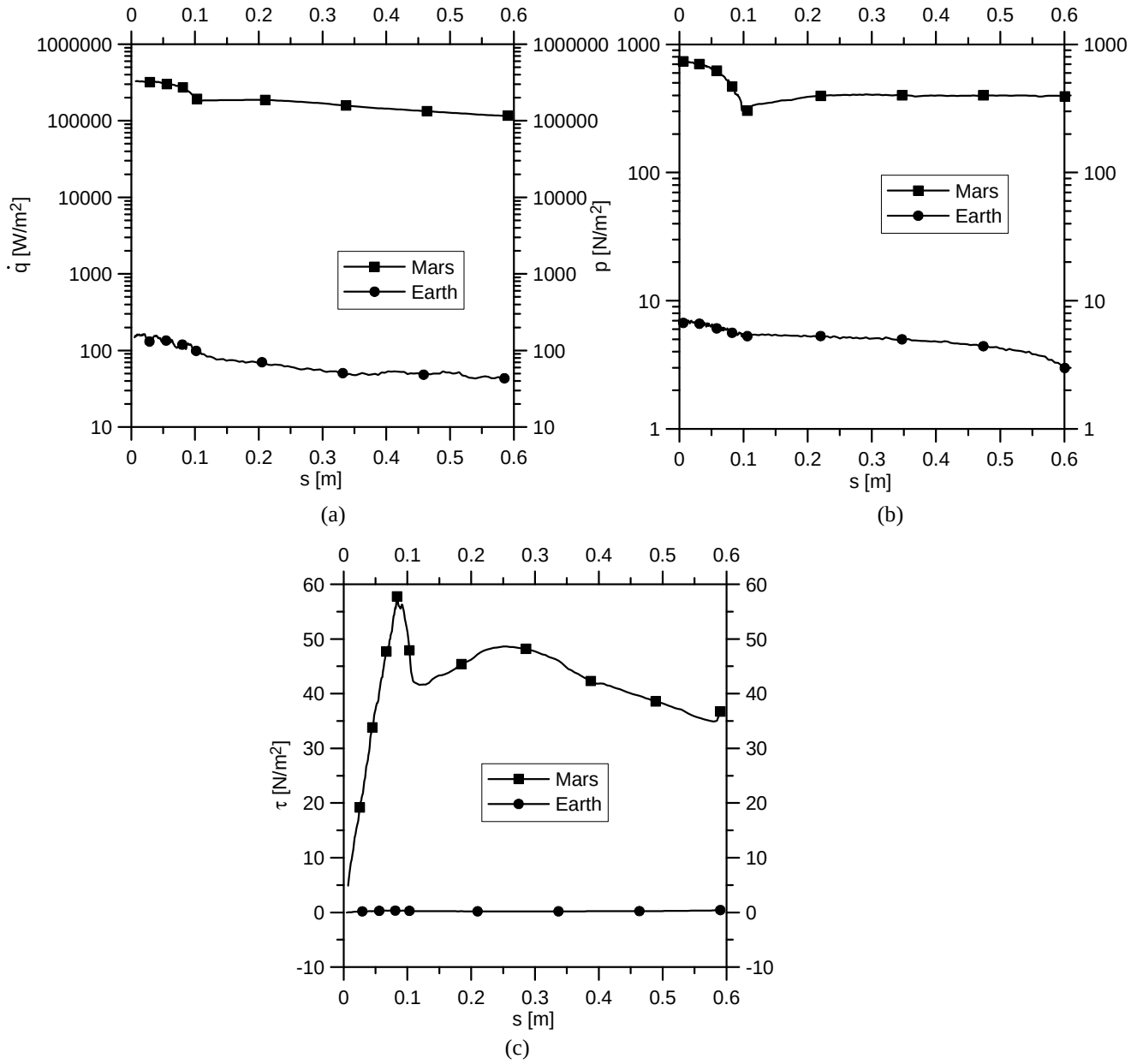

Fig. 6 – Profiles of heat flux (a), pressure (b) and skin friction (c) along the capsule surface: h=80 km

6.2 3-D tests

Considering that the beginning of the re-entry and/or entry is the most delicate phase, the stability analysis has been carried out at high altitude: h=96 and 80 km for Earth (these tests were already run to get the results presented in [1]) and h=100 and 80 km for Mars. Taking into account the reference system shown in Fig.1, a negative longitudinal moment indicates a nose-down pitching moment. Thus, the conditions $C_{Mz}=0$ (C_{Mz} is the longitudinal moment coefficient) and a negative value of the stability derivative $dC_{Mz}/d\alpha<0$ identify a stable equilibrium; the more negative the derivative, the more stable the equilibrium of the system.

The moment coefficients are computed considering as reference length the longitudinal dimension and as reference area the base area of the deployed aero-brake. The positions of the moment reduction pole for all tests, are

the points A and B (Fig.1) laying along the axis: x_A=0.1 m, x_B=0.15 m. These points identify possible positions of the gravity center.

Figures 7(a) to 7(d) show the profiles of C_{Mz} as functions of the angle of attack in the interval 0-10 deg or in direct (or nominal) attitude (Figs.7(a) and 7(b)) and in the interval 170-180 deg or in reverse attitude (Figs.7(c) and 7(d)). Figures 7(a) and 7(b) clearly verify that:

i) the capsule is longitudinally stable in direct attitude, i.e. around zero angle of attack,

ii) the position of the gravity center, along the capsule axis, influences the equilibrium stability; the more advanced this position the more stable the equilibrium,

iii) the stability is higher for Mars entry. This is probably due to the strong difference of the aerodynamic conditions (Mach and Reynolds numbers) and, more specifically, to the rarefaction level of the two flow fields (ratios Mach/Reynolds and Knudsen numbers, see Tables 3 and 4).

It seems that the lower the rarefaction level (or the smaller the ratio Mach/Reynolds and the Knudsen number, $Kn_{\infty D}$) the more stable equilibrium. This involves that the capsule is stable in reverse attitude or at α=180 deg (see Figs.7(c) and 7(d)) at h=100 km in the Mars entry. This condition is unfavorable because the capsule is not self-stabilizing). On the contrary, the rarefaction level at h=96 km for Earth re-entry is not sufficient to make the longitudinal equilibrium stable in reverse attitude.

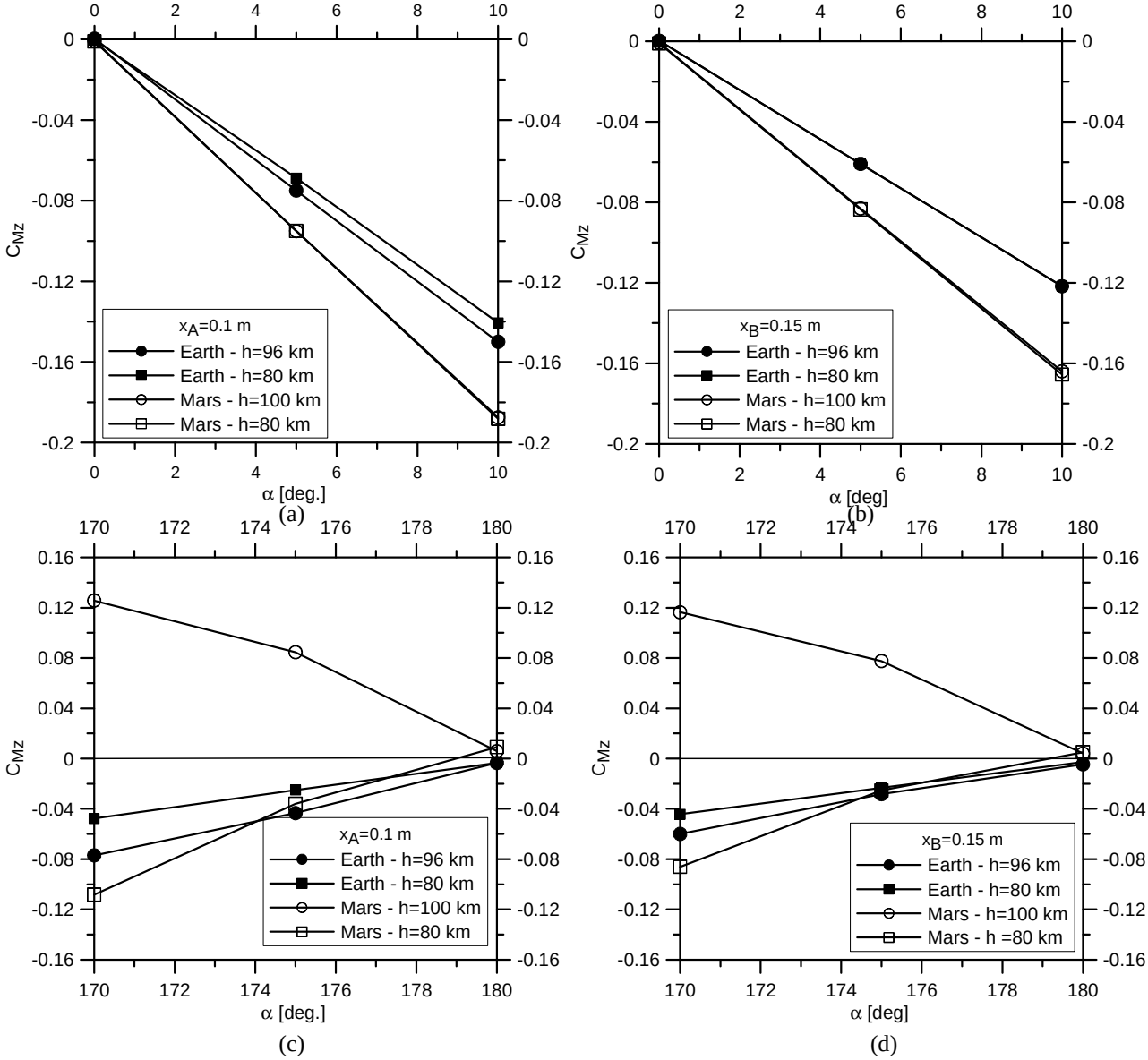

Fig. 7 – Profiles of longitudinal moment coefficient as function of the angle of attack

The values of the stability derivatives are reported in Tables 7 and 8 for the direct and reverse attitude, respectively. The computation of $dC_{Mz}/d\alpha$ [1/deg] was carried out at the angles of attack of 0, 5 and 10 deg for the nominal equilibrium condition around zero angle of attack and at the angles of attack of 170, 175 and 180 deg for the equilibrium condition around 180 deg angle of attack. The stability derivatives have been approximated by the slope of a least square straight line, interpolating the three coefficients of moments.

Table 7 – Stability derivatives [deg^{-1}] of the capsule in direct attitude (α=0 deg)

Earth	h=96 km, x_A	h=80 km, x_A	h=96 km, x_B	h=80 km, x_B
	-0.01503	-0.01403	-0.01220	-0.01220
Mars	h=100 km, x_A	h=80 km, x_A	h=100 km, x_B	h=80 km, x_B
	-0.01868	-0.01872	-0.01633	-0.01646

Table 8 – Stability derivatives [deg^{-1}] of the capsule in reverse attitude (α=180 deg)

Earth	h=96 km, x_A	h=80 km, x_A	h=96 km, x_B	h=80 km, x_B
	0.00735	0.00443	0.00554	0.00415
Mars	h=100 km, x_A	h=80 km, x_A	h=100 km, x_B	h=80 km, x_B
	-0.01198	0.01173	-0.01173	0.00912

For speculative purpose, the stability analysis for Mars entry at h=100 km has been continued considering two extra, even though improbable, positions of the gravity center: x=0.05 m, x=0.2 m. Figures 8(a) and 8(b) show the profiles of C_{Mz} in direct (a) and in reverse (b) attitude. As expected, a forward/backward movement of the gravity center increases/decreases the stability (the values of $dC_{Mz}/d\alpha$ are reported in Table 9). Unfortunately, the backward movement of the gravity center does not produce an instable equilibrium in reverse attitude.

Changing the aero-brake aperture angle is a possible solution of this problem. Probably, increasing this angle at values higher than 45 deg will involve a decrease of the stability derivative in direct attitude and an increase of the derivatives in reverse attitude; certainly, the optimal angle will be that keeping $dC_{Mz}/d\alpha$ negative in the direct attitude and making $dC_{Mz}/d\alpha$ positive in the reverse attitude.

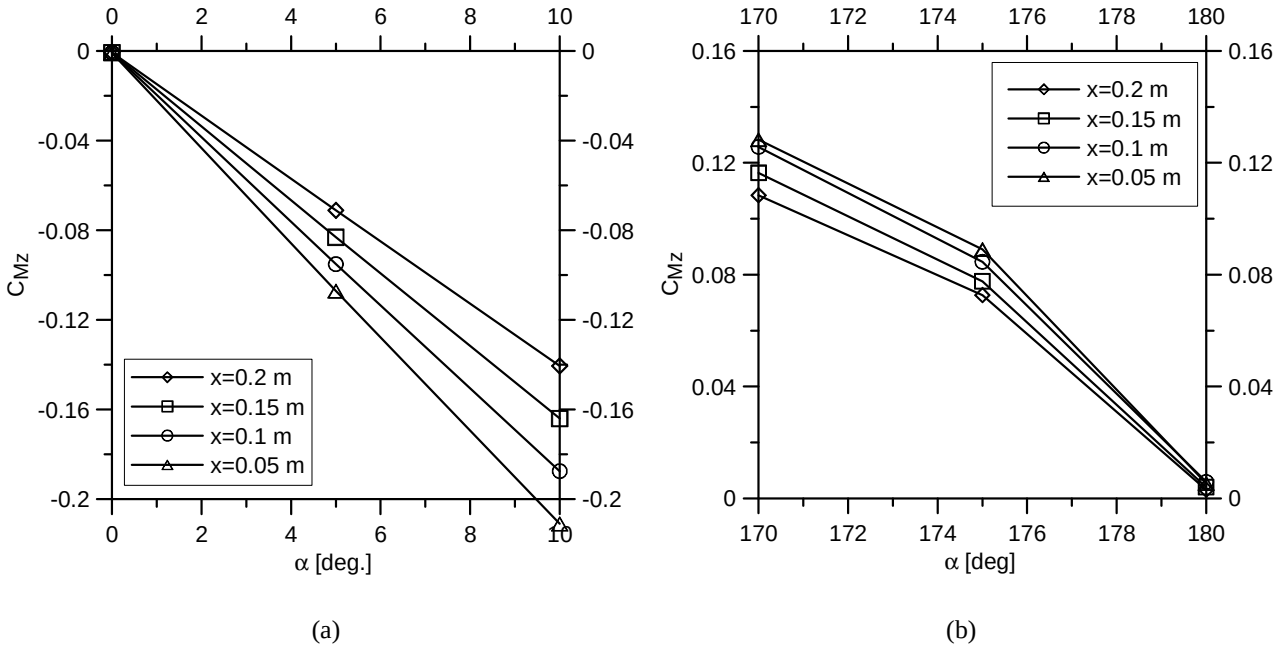

(a) (b)

Fig. 8 – Profiles of longitudinal moment coefficient as function of the angle of attack: Mars entry, h=100 km

Table 9 - Stability derivatives [deg^{-1}] of the capsule in direct (α=0 deg) and inverse (α=180 deg) attitudes at h=100 km

	x=0.05 m	x=0.2 m
α=0 deg	-0.02102	-0.01399
α=180 deg	-0.01229	-0.01053

8. Conclusions and further developments

The deployable, or umbrella like, re-entry capsule, thanks to lightness and to low costs of construction and of management seems to be a viable alternative to the current "conventional" capsules. The present authors already did successful computer tests, simulating the Earth re-entry of such a kind of capsule. In the perspective of an use of this type of capsule for the entry into the atmosphere of other planets, in the present study the dynamic and aerodynamic behaviors of the same capsule have been simulated during the Mars entry.

The present tests have been aimed at providing preliminary information about global parameters, such as drag coefficient, pitching moment and therefore at evaluating the longitudinal stability and local quantities such as heat flux, pressure and skin friction. The present analysis addressed also the consequences of the differences between Earth and Mars atmospheric properties and to the different trajectories, corresponding to ballistic, sub-orbital flight for Earth and direct entry into Mars atmosphere.

Due to much higher entry velocity, heat flux, pressure and shear stress at similar altitudes are several orders of magnitude higher for the entry into Mars atmosphere.

As further development of this study, a number of DSMC simulations have been already scheduled to investigate the effect of the aero-brake aperture angle and the basins of attraction of the stable equilibrium attitudes (forward and backward) by extending the simulations at larger angles of attack intervals (10-90 deg in direct attitude, 90-170 deg in reverse attitude).

9. References

[1] M. Iacovazzo, V. Carandente, R. Savino, G. Zuppardi, "Longitudinal Stability Analysis of a Suborbital Re-entry Demonstrator for a Deployable Capsule", Acta Astronautica, Vol. 106, Jan. 2015, pp 101-110

[2] L. Altenbuchner, J. Ettl, M. Horschgen, W. Jung, R. Kirchhartz, A. Stamminger, P. Turner, "MORABA-Overview on DLR's Mobile Rocket Base and Projects", Proceedings of the SpaceOps 2012 Conference, Stockholm (Sweden), 11-15 June 2012

[3] J.N. Moss, "Rarefied Flows of Planetary Entry Capsules", Special course on "Capsule Aerothermodynamics", Rhode-Saint-Genèse, Belgium, AGARD-R-808, 95-129, May 1995

[4] M.W. Tauber, A Rewiev of High Speed, Convective, Heat Transfer Computation Methods, NASA TP 2914, 1989

[5] EuroLaunch, Rexus User Manual V7.11, 8 January 2014

[6] MISTRAL Research Project: Proposal for the Aerospace Campania District, DAC Feasibility study, 2012.

[7] Charles-Campbell "Mars Entry, Descent and Landing"

[8] R.D. Braun, R.M. Manning, "Mars Exploration Entry, Descent and Landing Challenges", IEEE-2006-0076

[9] G. A. Bird, Molecular Gas Dynamics and Direct Simulation Monte Carlo, Clarendon Press, Oxford, Great Britain (1998).

[10] G. A. Bird, The DSMC Method, Version 1.1, Amazon, ISBS 9781492112907, Charleston, USA (2013)

[11] C. Shen, Rarefied Gas Dynamic: Fundamentals, Simulations and Micro Flows, Springer-Verlag, Berlin, Germany (2005)

[12] G.A. Bird, The DS2V Program User's Guide Ver. 3.3, G.A.B. Consulting Pty Ltd, Sydney, Australia (2005).

[13] G.A. Bird, The DS2V Program User's Guide Ver. 4.5, G.A.B. Consulting Pty Ltd, Sydney, Australia (2008)

[14] G.A. Bird, The DS3V Program User's Guide Ver. 2.6, G.A.B. Consulting Pty Ltd, Sydney, Australia (2006).

[15] R.N. Gupta, J.M. Yos, R.A. Thompson, "A Review of Reaction Rates and Thermodynamic Transport Properties for an 11-Species Air Model for Chemical and Thermal Non-Equilibrium Calculations to 30,000 K", NASA TM 101528 (1989).

[16] G.A. Bird, Sophisticated Versus Simple DSMC, Proceedings of the 25th International Symposium on Rarefied Gas Dynamics, edited by M. Ivanov and A. Rebrov, Saint Petersburg, Russia (2006).
[17] G.A. Bird, M.A. Gallis, J.R. Torczynski, D.J. Rader, *Phys Fluid.* **21**, 017103 (2009).
[18] M.A. Gallis, J.R. Torczynski, D.J. Rader, G.A. Bird, *J. Comput. Phys.* **228**, 4532-4548 (2009